

Model Predictive Control of Solar-Based Electric Vehicle Charging using a Quadratic Bidirectional Buck/Boost Converter (QBBC)

G. Divya¹, Dr. Venkata Padmavathi S.²

Submitted: 30/12/2023 Revised: 06/02/2024 Accepted: 14/02/2024

Abstract: An Electric Vehicle (EV) setup with an onboard PV array is introduced in this work, integrating an advanced Model Predictive Control system depending on Artificial Neural Network (ANN). The setup comprises a fuel cell, an electrolyzer, and an onboard PV array. The PV cell's role is to support the fuel cell by supplying power when sufficient irradiation is available. During the vehicle's idle state, the PV-generated power is directed to the electrolyzer, converting it into chemical energy. The produced hydrogen is then stored in the hydrogen tank. A quadratic bidirectional buck-boost converter is employed to fulfill the voltage needs of the motor and energy sources. The system is subjected to thorough analysis under various irradiance and speed conditions. To enhance the efficiency and economic feasibility of the PV system, a Maximum Power Point Tracking (MPPT) algorithm is used to obtain the highest available power commencing the PV panel. The system incorporates an enhanced incremental conductance algorithm for MPP. The control strategy encompasses both outer voltage and inner current control, efficiently regulating the DC output voltage of the quadratic bidirectional buck-boost converter. The vehicle drive utilizes an indirect vector-controlled induction motor. ANN-based Model Predictive Control (MPC) is employed to regulate the motor's speed. The paper introduces a novel approach for predictive torque control of AC machines, eliminating the need for weighting factors. To estimate the motor speed, an ANN estimator is employed. The equation for the predicted stator current is redefined and repositioned in accordance with the control procedure and ANN structure. MATLAB/SIMULINK is employed for simulations to assess the performance of the proposed EV configuration.

Keywords: Electric Vehicle, onboard PV array, DC-DC converter, Vector control, Induction motor

1. Introduction

The transportation sector holds immense importance in contemporary society. Despite the environmental challenges linked to their extensive usage, a notable reduction in the quantity of vehicles on transportation seems unlikely in the foreseeable future [1]. To address heightened pollution levels, especially in major cities, many countries have enacted severe regulations regarding the adoption of ICE vehicles. In response to these strict regulations, leading vehicle manufacturers are increasing their investments in the development and market introduction of various electric vehicles like fully EVs, fuel cell electric vehicles (FCEVs), plug-in hybrid (PHEV), and hybrid vehicles (HEV) [2]. Considerable research has been

conducted out in the realm of automotive electrification to improve the efficiency, performance, safety, reliability, and commercial feasibility of EVs. In recent years, research on EVs has primarily focused on several aspects, such as optimizing strategies related to electric motors, motor drives (including the DC-DC converter), and energy storage devices [3-5]. Furthermore, research has explored the design and sizing of powertrain components [6], optimal control strategies [7], applications and control strategies for hybrid vehicles to achieve a wide speed range [8], as well as aspects concerning battery chargers and grid charging management [9], [10], buck-boost DC/DC and bidirectional AC/DC converters, among other areas [11].

Electric vehicles (EVs) were introduced in the 19th century. However, their widespread adoption was hindered by factors such as high cost, limited range per charge, low speed, and lengthy charging times. Recent technological advancements have markedly enhanced EVs, boasting increased range per kilometer, reduced charging times, and higher speed capabilities. These improvements have rendered EVs more attractive to

1Ph.D Scholar, GITAM School of Technology, GITAM Deemed to be University, Hyderabad, Telangana & Assistant Professor / EEE, CVR College of Engineering, Hyderabad, Telangana

ORCID ID: 0000-0003-3320-0060

2Assistant Professor / EEE, GITAM School of Technology, GITAM Deemed to be University, Hyderabad, Telangana

ORCID ID: 0000-0001-8792-2152

** Corresponding Author Email: divya.gongidi@gmail.com*

consumers, particularly due to their zero-emission characteristics. Nevertheless, the introduction of EVs in India encounters a significant challenge posed by the insufficient charging infrastructure [12,13]. The progress of EV growth in India over the past decade is elaborated below [14].

- VIKRAM, the inaugural electric vehicle developed and manufactured in India, was introduced by Scooters India Pvt. Ltd.
- In 1999, Mahindra Ltd. developed Bijlee, a three-wheeler rickshaw. • In the year 2000, BHEL manufactured an 18-seater electric bus.
- Starting from 2001, REVA, an electric car, was marketed in India by a US firm.
- Hero Electric bikes, developed in partnership with the ULTRA Motor Company, were introduced and sold in 2007.
- Between 2008 and 2012, several companies, including Hyundai, Toyota, TATA Motors, Maruti Suzuki, Ashok Leyland, among others, entered the Indian market to stimulate the manufacture and sales of electric vehicles.
- The "National Electric Mobility Mission Plan (NEMMP) 2020," implemented from 2012 to 2020, aimed to promote EVs and make sure national fuel security.

Investors in electric vehicles are eagerly anticipating a surge in EV adoption on the streets, which they believe will precede significant advancements in charging facilities. Additionally, the general public's willingness to purchase EVs is heavily reliant on the availability of multiple charging options.

Currently, in India, the rate of electricity required to charge an electric vehicle is only a small portion of the cost of petrol required to travel the same distance. However, charging multiple EVs simultaneously using a conventional power grid poses significant challenges. Hence, it's important to upgrade the power system by integrating energy storage and renewable energy sources to meet sustainable power needs. Key features of combining energy storage with renewable energy systems include ensuring a reliable energy supply, storing energy for future use, boosting efficiency, increasing the capacity of power generation, and maintaining stable power quality by reducing fluctuations.

In an FCHEV, the primary power comes from a fuel cell pack, that works alongside another ESS to run the

vehicle's electric motor. The benefit of this setup over traditional hybrid vehicles or those with internal combustion engines is that it uses an electric motor as an alternative to ICEs. This shift enhances efficiency and minimizes environmental effects. A plug-in hybrid electric vehicle (PHEV) includes an ICE to increase its driving range. An FCEV offers benefits such as enhanced efficiency, decreased air pollution, use of affordable clean energy sources, and versatility for different industrial uses. Electric power is produced by a fuel cell using hydrogen, oxygen, and an electrolyte in a chemical reaction. Among different fuel cell systems, proton exchange membrane fuel cell (PEMFC) technology stands out for vehicles because of its higher power generation density and lower heat production, which improves overall efficiency.

The main drawback of employing a fuel cell in a vehicle is its limited ability to react to rapid changes quickly and efficiently in the EV's power demand [24]. The fuel cell stack finds it challenging to promptly adjust to unexpected increases or reductions in power demand, such as those required for acceleration. Furthermore, the fuel cell stack also struggles to store regenerative power generated during deceleration and braking. Therefore, an additional ESS, like a battery or supercapacitor bank, becomes necessary. These extra storage devices, with suitable capacity and quick response times, should be used alongside the fuel cell stack as auxiliary energy storage. This paper introduces a new electric vehicle setup managed by Model Predictive Control (MPC). The setup comprises a fuel cell, electrolyzer, and PV cell. When there's enough sunlight, the onboard or rooftop PV array can support the fuel cell in producing power. Additionally, when the vehicle is not in use, the PV system can turn the generated power into chemical energy using electrolyzer. The produced hydrogen can then be collected in a designated hydrogen tank.

In this study, a quadratic bidirectional buck-boost converter is used to meet the voltage needs of the motor and energy sources. The motor speed is regulated using ANN MPC, which employs a unique approach for predictive torque control of AC machines without requiring weighting factors. An ANN estimator predicts the motor's speed, and the equation for the predicted stator current is formulated and adjusted according to the regulating process and ANN structure. To improve the accuracy of motor speed prediction, the weight dependent on speed in the ANN is adjusted using the Windrow-Hoff optimization rule. This reduces the sum of squared errors between the measured stator current and the predicted stator

current obtained from the ANN output. The speed estimation is based on the mentioned weight, significantly improving online speed estimation capabilities while maintaining a simple ANN structure. The quadratic bidirectional buck-boost converter in the system ensures a steady and enhanced voltage across the DC terminals of the motor's inverter. The proposed EV setup is tested under different levels of sunlight and varying speeds. Section 2 describes the suggested EV setup, Section 3 delves into the fuel cell and electrolyzer, Section 4 addresses the indirect vector control of the induction motor, and Section 5 details the model predictive control and ANN estimation of the motor's speed. The simulation outcomes are outlined in Section.

2. Electric Vehicle with Solar Onboard

To maintain a consistent and cost-effective power supply, we require energy storage solutions, despite potential impacts on reliability and availability. However, each option comes with its own set of advantages and difficulties. Combining the benefits of solar energy and fuel cells in Hybrid Electric Vehicles can make them more efficient and reliable. Figure 1 shows a common setup of an Electric Vehicle with both onboard solar and fuel cell.

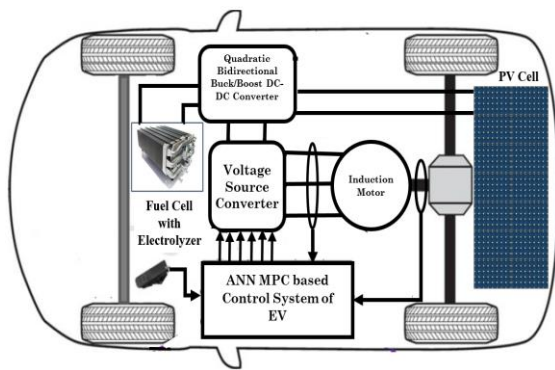


Fig 1. Onboard PV Hybrid Electric Vehicle

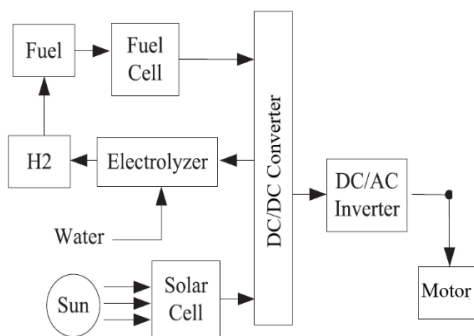


Fig 2. HEV with Solar and Fuel Cell

HEVs use DC-DC bidirectional boost-buck converters, which can handle power flow in both directions. Boost converters with high gain are gaining attention in power electronics research because they're increasingly needed in various applications. Conventional boost converters encounter difficulties in reaching a high step-up gain. Because of this, there's a need for converters that have both high gains and efficiency to overcome these limitations. One way to increase the voltage gains of a converter is by adjusting its duty cycle or increasing the turns ratio of the coupled inductor. However, a common problem with these converters is that they cause a lot of ripples in the input current. Quadratic converters have become quite popular among power electronics researchers because they provide a method to increase the gain of regular boost converters while also dealing with some of the drawbacks of other methods.

2.1. Electrolyzer

The Unipolar cell is known for being efficient with low maintenance needs and strong reliability. It works by each electrode having only one polarity, which leads to the production of H_2 (cathode) or O_2 (anode). The electrolyzer consists of several cells, each contained within its own compartments. Under typical operating conditions, the cell voltages range from 1.7 to 1.9 volts. The electrolyzer operates at temperatures below 70°C , which helps alleviate material constraints. H_2 is produced with 99.9% purity, and the efficiency is 100%, guaranteeing a high level of hydrogen generation.

$$X_{H_2} = \frac{5.18e^{-6}I_e \text{mole}}{s} \quad (1)$$

The electricity flowing between the electrodes (I_e) helps store (H_2) at a pressure of 3 bars in a tank. This stored hydrogen is used to power the motor when sunlight is low and is then supplied to the fuel cell (FC).

2.2. Fuel cell

The Nernst equation is a fundamental equation in electrochemistry that relates the electromotive force (EMF), or voltage, of an electrochemical cell to the standard electrode potential, temperature, and concentrations of the species involved in the redox reaction. The Nernst equation allows us to calculate the cell potential under non-standard conditions, considering variations in temperature and concentration. It demonstrates how changes in concentration can affect the voltage of an

electrochemical cell and provides insights into the thermodynamics of electrochemical reactions.

$$V_o = E_o + \frac{R \cdot T}{2F} \ln \left(\frac{x_{H_2} x_{O_2}}{x_{H_2O}} \right)^{0.5} \quad (2)$$

3. Quadratic Bidirectional Boost/Buck DC-DC Converter

Figure 3 displays a diagram of the Quadratic Bidirectional Boost/Buck DC-DC converter [29]. This design differs from the typical Boost quadratic converter. Unlike the traditional version, this setup doesn't need additional passive components like inductors and capacitors in the power circuit. It keeps a steady voltage gain, which follows a quadratic function in both Boost and Buck modes. Using just one switch, the converter either charges or discharges. It works in two modes: Boost and Buck. In the forward mode, the converter operates like a Boost converter, transferring energy from the input to the output. Two IGBTs (T1 and T4) are always off, while IGBT T3 remains on continuously. By employing PWM with a switching time of T_c , output voltage and the inner current for IGBT T2 are regulated. During the time interval ΔT_s , when IGBT T2 is turned on, inductors L1 and L2 gradually charge with a current that rises continuously, transferring energy from capacitor C to inductor L2. On the other hand, during the time interval $1-\Delta T_s$, when IGBT T2 is activated, inductors L1 and L2 discharge energy with a current that gradually diminishes. This process transfers energy from input to output through the inductors and the capacitor.

During Boost Mode

$$\Delta V_{in} + (1 - \Delta)(V_{in} - V_c) = 0 \quad (3)$$

$$\Delta V_c + (1 - \Delta)(V_c - V_{out}) = 0 \quad (4)$$

Then voltage gain is given as

$$G = \frac{V_{out}}{V_{in}} = \frac{1}{(1 - \Delta)^2} \quad (5)$$

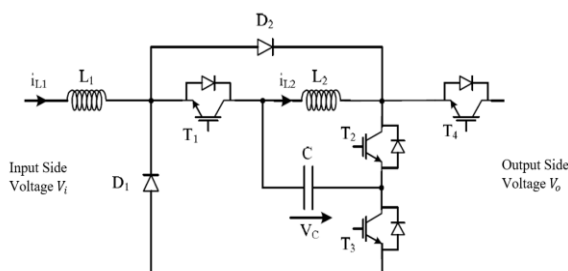


Fig 3. QBBC DC-DC converter

When working as a Buck converter, the main goal of the converter is to move power from the output side to the input side. IGBTs T2 and T3 are always deactivated, while T4 stays activated. By using PWM with a switching time of T_c , it regulates T1 to control the output voltage and inner current. During the time ΔT_s , when T1 is switched on, the currents in inductors L1 and L2 rise as capacitor C releases its energy, transferring it to inductor L1. When T1 is turned off, the currents in inductors L1 and L2 decrease, and the energy stored in the inductors moves to capacitor C and goes back to the input side of the converter.

In Buck Mode

$$\Delta(V_c - V_{in}) - (1 - \Delta)V_{in} = 0 \quad (6)$$

$$\Delta(V_c - V_{out}) + (1 - \Delta)V_c = 0 \quad (7)$$

Then voltage gain is given as

$$G = \frac{V_{in}}{V_{out}} = \Delta^2 \quad (8)$$

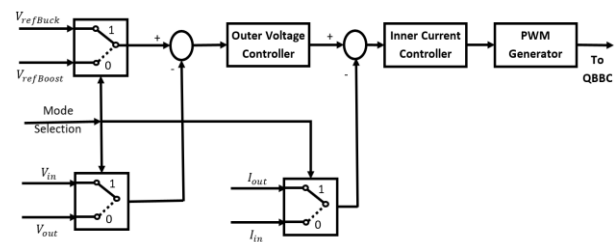


Fig 4. Control Strategy for QBBC

In Figure 3, it can see the control setup for the bidirectional DC-DC converter, which handles both buck and boost modes. The mode selection depends on the power flow or direction of current, allowing the converter to switch between buck and boost modes as needed. Incorporating the DC-DC converter involves setting up two loops: one to maintain voltage stability and another to control the current. This arrangement employs PI controllers to regulate both voltage and current.

4. Indirect vector control of induction motor for electric vehicle

Selecting an induction motor for the electric vehicle drive is due to its reliable performance in different conditions, simple construction, long-lasting durability, minimal maintenance needs, and reasonable commercial cost. As there are no brushes, friction losses are minimized, which means there are fewer restrictions on reaching the highest possible speed. This allows for an increase in maximum speed while still maintaining a high output of mechanical power. Adjusting the frequency of the input voltage

Then

$$r_r i_{qr} + \omega_{sl} \lambda_r = 0 \quad (24)$$

$$r_r i_{dr} + \frac{d\lambda_{dr}}{dt} = 0 \quad (25)$$

$$i_{qr} = \frac{-L_m}{L_r} i_{qs} \quad (26)$$

$$i_{dr} = \frac{\lambda_r - L_m i_{ds}}{L_r} \quad (27)$$

the rotor currents from the equations,

$$i_f = \frac{1}{L_m} [1 + T_r P] \lambda_r \quad (28)$$

$$\omega_{sl} = -\frac{r_r i_{qr}}{\lambda_r} = \frac{L_m i_T}{T_r \lambda_r} \quad (29)$$

Where

$$i_T = i_{qs}, i_f = i_{ds}, T_r = \frac{L_r}{r_r}, K_{te} = \frac{4}{3P} \quad (30)$$

Using the substituted rotor currents, the torque can be expressed as:

$$T_e = \frac{3P L_m}{4 L_r} (\lambda_{dr} i_{qs} - \lambda_{qr} i_{ds}) = \frac{3P L_m}{4 L_r} \lambda_{dr} i_{qs} = K_{te} \lambda_r i_{qs} \quad (31)$$

Equation (31) demonstrates that the torque is affected by both the rotor flux linkages, λ_r , and the stator q-axis current, i_{qs} . Hence, the rotor flux linkage constant, the torque becomes dependent on the stator current. The stator current phasor is obtained by combining the stator currents along the 'd' and 'q' axes in any reference frame, expressed as:

$$|i_s| = \sqrt{(i_{qs})^2 + (i_{ds})^2} \quad (32)$$

In the indirect vector control system, the motor speed and input currents are measured, and this information is then sent back to the controller as feedback. This generates reference currents. In Figure 5, a PI controller uses the speed error as input to create the reference torque. This torque reference is then fine-tuned to reduce the gap between the reference speed and the actual speed. To calculate the reference flux using the field weakening technique, it utilizes the motor's speed, and the expression can be stated as:

$$\lambda_r^* = \begin{cases} \lambda_b & \text{if } 0 \leq |\omega_r| \leq \omega_{rated} \\ \frac{\omega_b}{|\omega_r|} \lambda_b & \text{if } \omega_b \leq |\omega_r| \leq \omega_{r(max)} \end{cases} \quad (33)$$

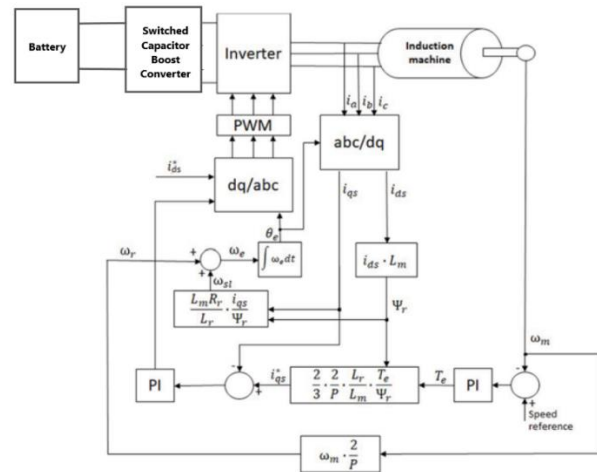


Fig 6. The implementation of vector control.

At the rated speed, the reference flux (λ_{ref}) is equal to the rated flux (λ_b) multiplied by the rated rotor speed (ω_r). When speeds go beyond the rated speed, the reference flux can be decreased to sustain a consistent power output.

5. Model Predictive Control

5.1. Inverter Model

In this study, it uses the two-level voltage source inverter (2L-VSI) shown in Figure 1. Despite producing a significant number of harmonics, this inverter is favoured because of its simplicity and versatile power conversion abilities. Each output leg of the 2L-VSI has only two power switches that work together. Figure 2 shows the eight voltage vectors created by the 2L-VSI. In these vectors, v_0 and v_7 are null voltage vectors, which means ($v_\alpha = 0$; $v_\beta = 0$).

The equations for the 2L-VSI are as follows:

$$v_a = S_a \frac{V_{dc}}{2} \quad (34)$$

$$v_b = S_b \frac{V_{dc}}{2} \quad (35)$$

$$v_c = S_c \frac{V_{dc}}{2} \quad (36)$$

The voltage in $\alpha - \beta$ frame can be as

$$\begin{bmatrix} v_\alpha \\ v_\beta \end{bmatrix} = \frac{2}{3} V_{dc} \begin{bmatrix} 1 & -0.5 & -0.5 \\ 0 & \sqrt{3}/2 & -\sqrt{3}/2 \end{bmatrix} \begin{bmatrix} S_a \\ S_b \\ S_c \end{bmatrix} \quad (37)$$

5.2. Motor Model

The mathematical model of the induction motor (IM) involves the state variables of stator flux (Ψ_s) and stator current (i_s). In a stationary frame, the dynamic equations of the IM can be expressed as follows:

$$v_s = r_s i_s + \frac{d\lambda_s}{dt} \quad (38)$$

$$0 = r_s i_r + \frac{d\lambda_r}{dt} - j \frac{\omega_r}{p} \lambda_r \quad (39)$$

$$\lambda_s = L_s i_s + L_m i_r \quad (40)$$

$$\lambda_r = L_m i_s + L_r i_r \quad (41)$$

$$T = \frac{3}{2} p |\lambda_s \otimes i_s| \quad (42)$$

$$j \frac{d\omega_r}{dt} = T_e - T_L \quad (43)$$

To forecast the torque and flux, it's vital to estimate the stator flux (λ_s) and the rotor flux (λ_r) at the current sampling time (k). It can find the rotor flux by using the right equation that describes the rotor dynamics of an induction motor (IM) in a rotating reference frame aligned with the rotor winding.

$$\psi_r + \tau_r \frac{d\psi_r}{dt} = L_m i_s \quad (44)$$

The rotor time constant $\tau_r = L_r/R_r$ is crucial. By employing the backward-Euler discretization with the sampling time (T_s), the discrete-time equation for estimating the rotor flux is expressed as follows:

$$\lambda_r^k = L_m \frac{T_s}{T_r} i_s^{k-1} + \left(1 - \frac{T_s}{T_r}\right) \lambda_r^{k-1} \quad (45)$$

The stator flux can be valued by

$$\lambda_s^k = \frac{L_m}{L_r} \lambda_r^k + \left(1 - \frac{L_m^2}{L_s L_r}\right) i_s^k \quad (46)$$

Now, the stator flux using the forward-Euler discretization:

$$\lambda_s^{k+1} = \lambda_s^k + T_s v_s^k - T_s R_s i_s^k \quad (47)$$

the stator current using the forward-Euler discretization:

$$i_s^{k+1} = C_1 i_s^k + C_2 \lambda_s^k + \frac{T_s}{L_\sigma} v_s^k \quad (48)$$

where $R_\sigma = (R_s + (L_m/L_r)^2 R_r)$ relates to the equivalent resistance, $C_1 = (1 - (R_\sigma T_s/L_\sigma))$, $L_\sigma = \sigma L_s$ is the leakage inductance of the system and

$$C_2 = \frac{(L_m/L_r) T_s}{L_\sigma ((1/\tau_r) - j\omega^k)} \quad (49)$$

Finally, expecting the torque varies on the forecasted values of stator flux and current, expressed as follows.

$$T^{k+1} = \frac{3}{2} p |\lambda_s^{k+1} \otimes i_s^{k+1}| \quad (50)$$

6. Online Artificial Neural Network Speed Estimator

From mathematical modeling of induction motor

$$\begin{bmatrix} v_{ds} \\ v_{qs} \\ 0 \\ 0 \end{bmatrix} = \begin{bmatrix} r_s + L_s \frac{d}{dt} & 0 & L_m \frac{d}{dt} & 0 \\ 0 & r_s + L_s \frac{d}{dt} & 0 & L_m \frac{d}{dt} \\ L_s \frac{d}{dt} & \omega_r L_m & r_r + L_r \frac{d}{dt} & \omega_r L_r \\ -\omega_r L_m & L_m \frac{d}{dt} & -\omega_r L_r & r_r + L_r \frac{d}{dt} \end{bmatrix} \begin{bmatrix} i_{ds} \\ i_{qs} \\ i_{dr} \\ i_{qr} \end{bmatrix} \quad (51)$$

Stator current can be estimated as

$$\frac{d}{dt} \begin{bmatrix} \hat{i}_{ds} \\ \hat{i}_{qs} \end{bmatrix} = \begin{bmatrix} -\frac{r_s^*}{L_\sigma} & -\omega_r & \frac{r_r}{L_\sigma L_r} & \frac{\omega_r}{L_\sigma} \\ \omega & -\frac{r_s^*}{L_\sigma} & \frac{\omega_r}{L_\sigma} & \frac{r_r}{L_\sigma L_r} \end{bmatrix} \begin{bmatrix} \hat{i}_{ds} \\ \hat{i}_{qs} \\ \hat{\lambda}_{ds} \\ \hat{\lambda}_{qs} \end{bmatrix} + \frac{1}{L_\sigma} \begin{bmatrix} v_{ds} \\ v_{qs} \end{bmatrix} \quad (52)$$

Using the forward rectangular rule and rearranging the resulting equation to be suitable for ANN implementation, the discrete-time estimation of the stator current is represented as:

$$\begin{bmatrix} \hat{i}_{ds}^k \\ \hat{i}_{qs}^k \end{bmatrix} = \left(1 - \frac{T_s r_s^*}{L_\sigma}\right) \begin{bmatrix} \hat{i}_{ds}^{k-1} \\ \hat{i}_{qs}^{k-1} \end{bmatrix} + \frac{T_s \omega_r}{L_\sigma} \begin{bmatrix} \hat{\lambda}_{sd}^{k-1} \\ \hat{\lambda}_{sq}^{k-1} \end{bmatrix} + \frac{T_s r_r}{L_\sigma L_r} \begin{bmatrix} \hat{\lambda}_{sd}^{k-1} \\ \hat{\lambda}_{sq}^{k-1} \end{bmatrix} + \frac{T_s}{L_\sigma} \begin{bmatrix} v_{ds}^{k-1} \\ v_{qs}^{k-1} \end{bmatrix} \quad (53)$$

This equation can be simplified as

$$\vec{i}_s^k = w_1 \vec{x}_1 + w_2 \vec{x}_2 + w_3 \vec{x}_3 + w_4 \vec{x}_4 \quad (54)$$

Where $w_1 = \left(1 - \frac{T_s r_s^*}{L_\sigma}\right)$, $\vec{x}_1 = \begin{bmatrix} \hat{i}_{sd}^{k-1} \\ \hat{i}_{sq}^{k-1} \end{bmatrix}$, $w_2 = \frac{T_s \omega_r}{L_\sigma}$, $\vec{x}_2 = \begin{bmatrix} \hat{\lambda}_{sd}^{k-1} \\ \hat{\lambda}_{sq}^{k-1} \end{bmatrix}$, $w_3 = \frac{T_s r_r}{L_\sigma L_r}$, $\vec{x}_3 = \begin{bmatrix} \hat{\lambda}_{sd}^{k-1} \\ \hat{\lambda}_{sq}^{k-1} \end{bmatrix}$, $w_4 = \frac{T_s}{L_\sigma}$ and $\vec{x}_4 = \begin{bmatrix} v_{ds}^{k-1} \\ v_{qs}^{k-1} \end{bmatrix}$

Equation (54) implies that the ANN consists of two layers—the input layer and the output layer. Therefore, the Widrow–Hoff learning rule is considered the appropriate learning procedure for this ANN configuration. This learning method offers a straightforward weight update equation, making it more suitable for online speed estimation compared to other learning methods. Therefore, the weight w_2 in Equation (54), which includes the speed, will be continuously modified online using the Widrow–Hoff optimization. This goal is to reduce the total of squared differences between the actual stator current and the estimated stator current. The sum of squared errors at sampling time k is shown by the energy function:

$$E = \frac{1}{2} \left((i_{sd}^k - \hat{i}_{sd}^k)^2 + (i_{sq}^k - \hat{i}_{sq}^k)^2 \right) \quad (55)$$

In Equation (54), only the weight w_2 is updated online. So, the accuracy of the estimated stator current largely depends on how well the estimated speed converges. A small learning rate results in slow convergence, while a large learning rate speeds up convergence but can cause fluctuations in the estimated speed. Therefore, it's crucial to choose the learning rate carefully to ensure stability in the estimation system.

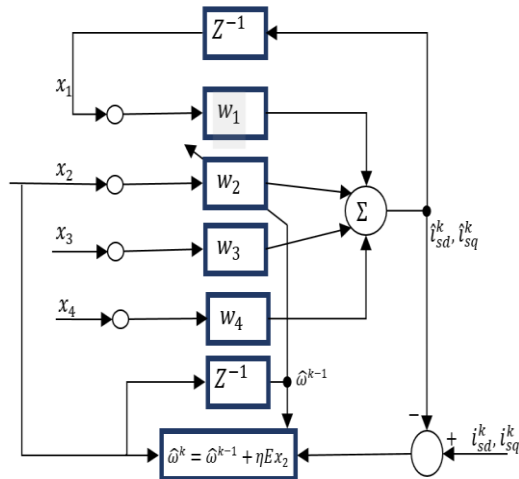


Fig 7. online artificial neural network (ANN) speed estimator

7. Simulink model of proposed system

The configuration of a hybrid electric vehicle equipped with an onboard PV array, controlled by an ANN-based MPC system, is simulated using MATLAB/SIMULINK to assess its performance. The simulated system is illustrated in Figure 1. The main power source for the electric vehicle is primarily a fuel cell, with an onboard solar cell serving as a secondary source. Also, energy generated during braking or deceleration is stored in a hydrogen tank by converting electrical energy into chemical energy through an electrolyzer.

To control motor speed, we use the indirect vector control technique, and then further regulate the speed using MPC. The MPC is adjusted specifically for motor speed control. An ANN is used to forecast the speed of the induction motor. To evaluate the suggested setup performance, the simulation considers variations in irradiation, speed, and torque.

CASE 1:

The evaluation of the proposed EV setup is carried out under changing speed conditions. The desired speed of the motor is increased from 100 rad/s to 120 rad/s at

10 seconds of the simulation. Meanwhile, the irradiation level stays steady at 1000 W/m², as shown in Figure 8.

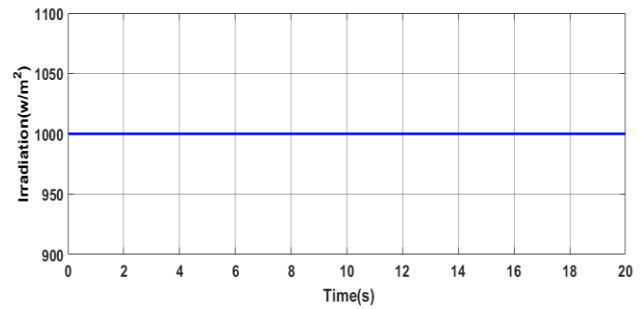
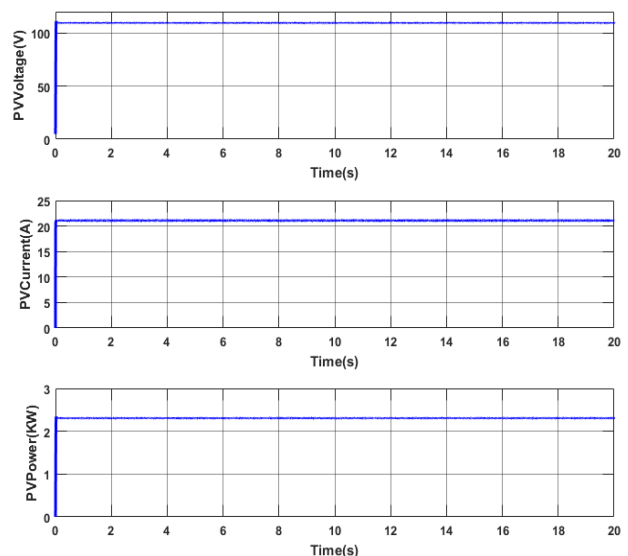
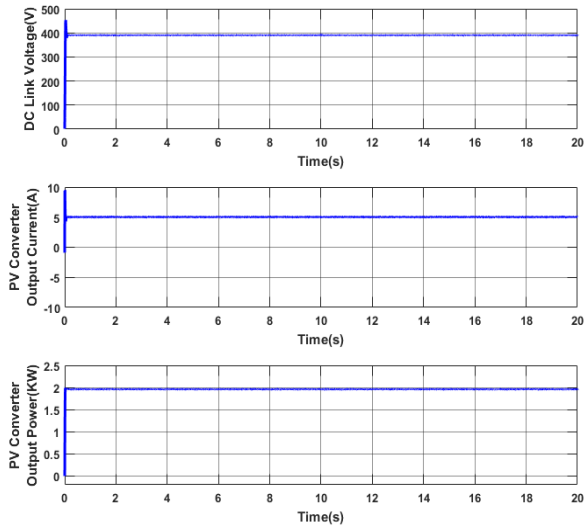


Fig 8. Irradiance of PV cells

The motor's reference speed remains at 100 rad/s until the 10-seconds, after which it is increased to 120 rad/s. Figure 9a shows the voltage, current, and power generated by the PV array under constant irradiation. To ensure resilience against changing atmospheric conditions, the Incremental Conductance algorithm is used for the MPPT. At an irradiation level of 1000 W/m², the PV cell produces 2.01 kW of power. Figure 9b shows the output voltage, current, and power of the PV converter. Also, Figure 10a displays the voltage, current, and power generated by the fuel cell, while figure 10b illustrates the voltage, current, and power of the fuel cell converter. Figure 11 illustrates the voltage, current, and power of the electrolyzer. Additionally, Figure 12(a) displays the input and output voltages of the QBBC converter.

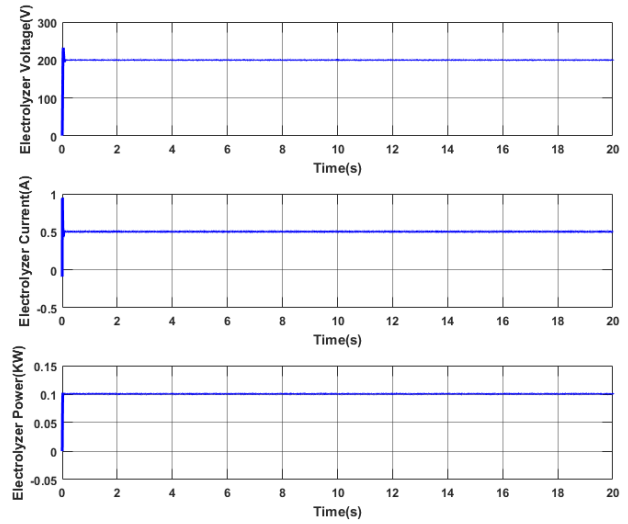


(a)

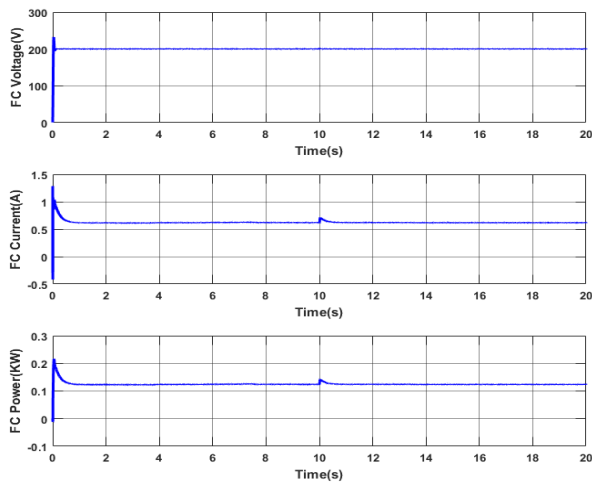


(b)

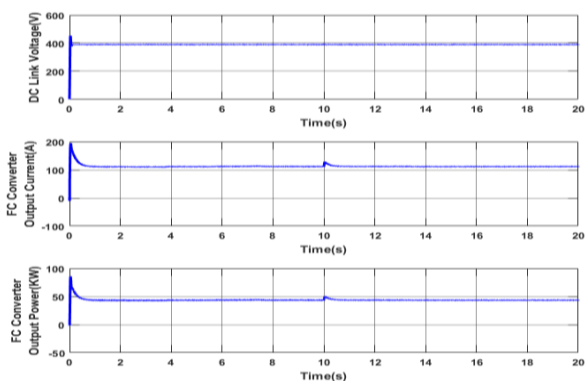
Fig 9. PV Cells Voltage and current (a) PV output voltage, current and power (b) PV converter output voltage, current and power



(a)

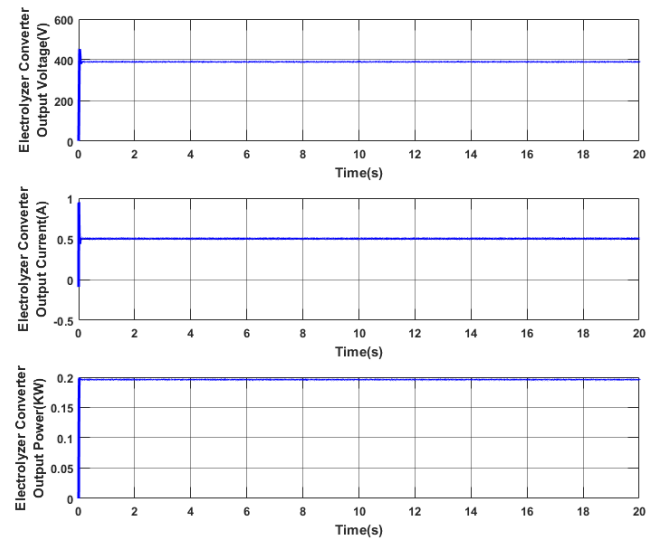


(a)



(b)

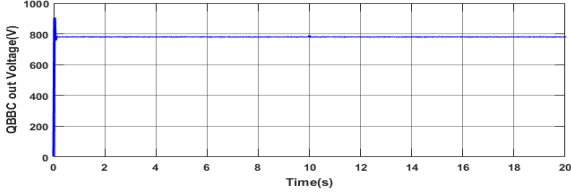
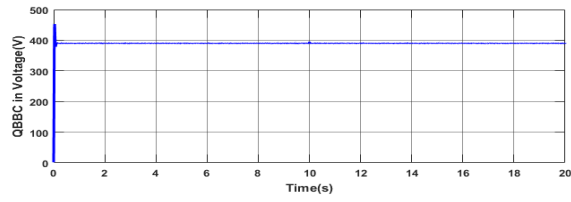
Fig 10. Fuel Cell Voltage and current (a) FC output voltage and power (b) FC converter output voltage, current and power



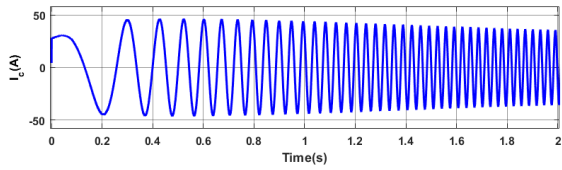
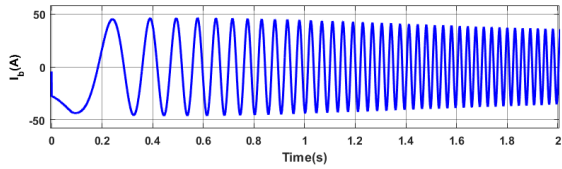
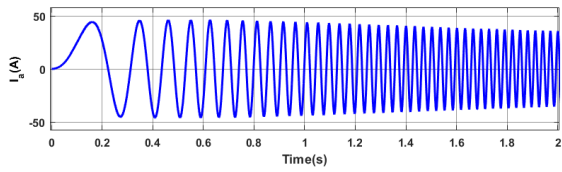
(b)

Fig 11. Electrolyzer Voltage and current (a) Electrolyzer voltage, current and power (b) Electrolyzer converter input voltage, current and power

The QBBC converter transfers the input voltage from 400V to 780V, which is crucial for the vehicle drive, by employing voltage and current loops. Fig 12(b) displays the three-phase stator currents of the motor with PI controller, and fig 14 demonstrates the stator current with the proposed ANN MPC control. Significantly, the THD in stator current decreases from 5.3% with PI control to 2.8% when adopting ANN MPC control for the motor. The speed and torque of the vehicle drive with PI control and ANN MPC control are shown in fig 13. The findings indicate that with ANN MPC control, peak overshoot, rise time, and stability time are minimized compared to PI control.

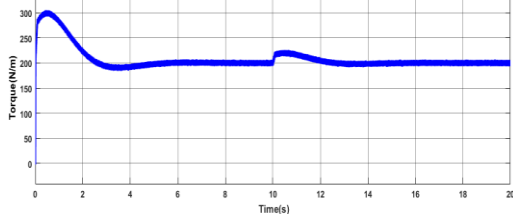
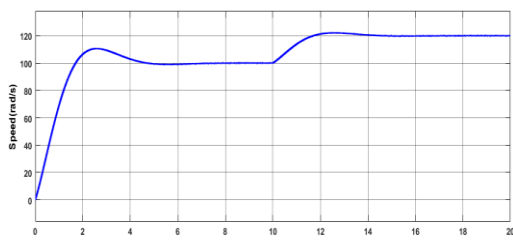


(a)

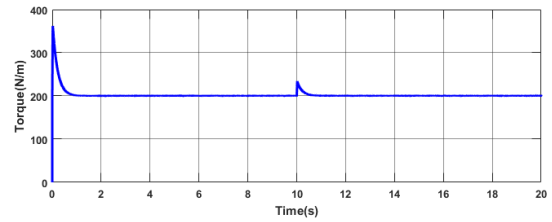
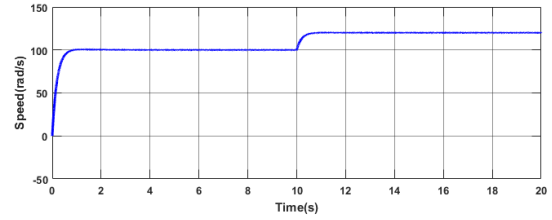


(b)

Fig 12. (a) QBBC input voltage and output voltage
(b) Motor Stator Currents during Starting with PI control



(a)



(b)

Fig 13. Motor Speed and Torque (a) with PI Control
(b) with Proposed Control

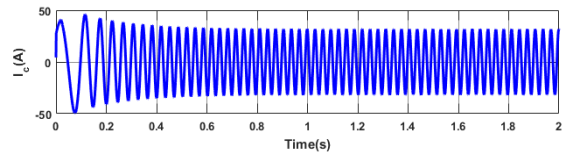
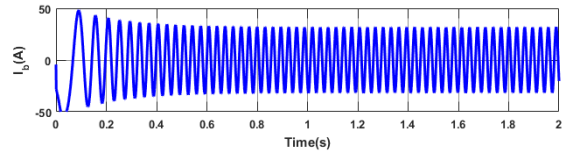
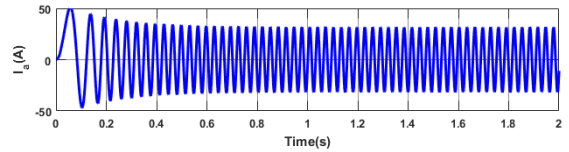


Fig 14. Motor Stator Currents during Starting with Proposed Control

CASE2:

The evaluation of the proposed EV setup is carried out under changing irradiation conditions. In this scenario, the reference speed for the vehicle drive's vector control rises from 100 rad/sec to 120 rad/sec at the 10-seconds. The irradiance changes as follows: it starts at 600 W/m², increases to 800 W/m² at the 3rd second, further rises to 1000 W/m² at the 6th second, decreases to 400 W/m² at the 9th second, and then increases again to 900 W/m² at the 12th second.

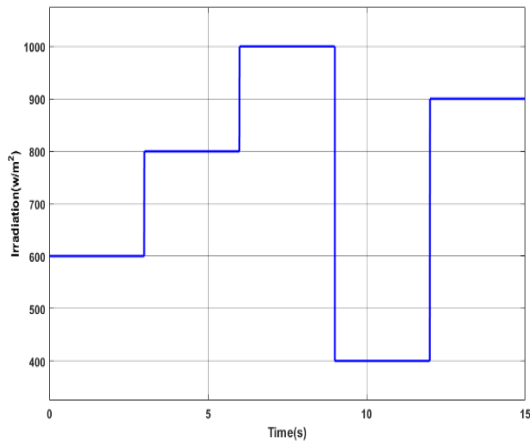
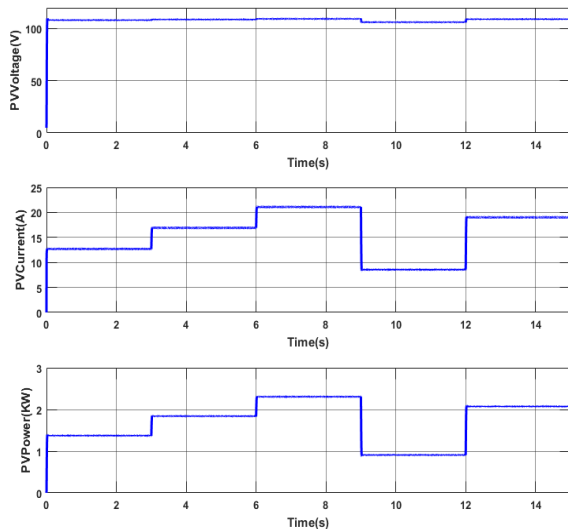
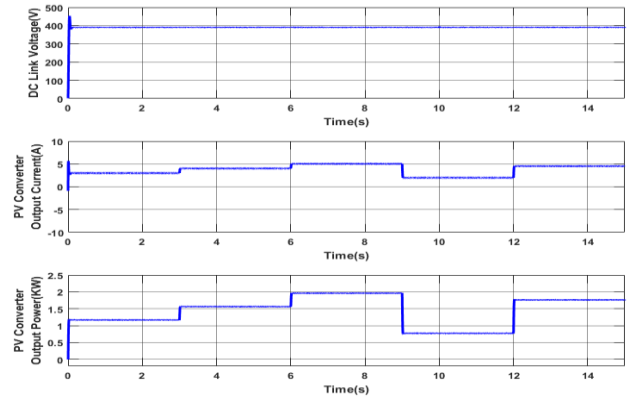


Fig 15. Irradiance of PV cells

The changing irradiance is shown in Figure 15. Figure 19(a) displays the input voltage and increased output voltage of the QBBC converter. The controlled and increased output voltage of the QBBC converter ensures that changes in the irradiance of the PV cell do not impact the output voltage supplied to the vehicle drive inverter. Figure 20 depicts the motor speed and torque under both PI control and the proposed control. Additionally, Figure 16 provides information about the output voltage, current, and power of the PV system and its boosting converter. Figure 17 displays the output voltage, current, and power of the fuel cell and its converter, while Figure 18 illustrates the voltage, current, and power of the electrolyzer and its converter.

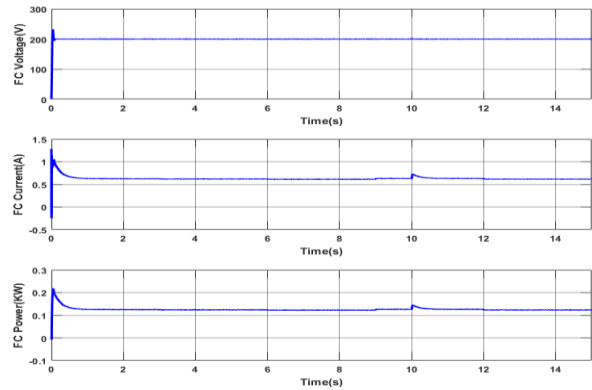


(a)

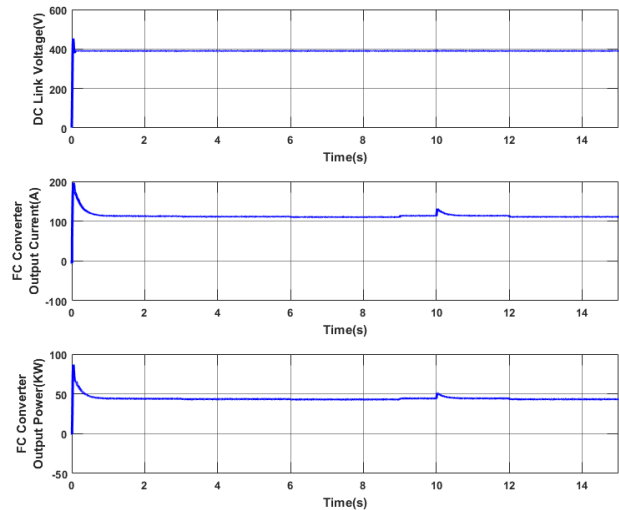


(b)

Fig 16. PV Cells Voltage and current (a) PV output voltage and power (b) PV converter output voltage, current and power

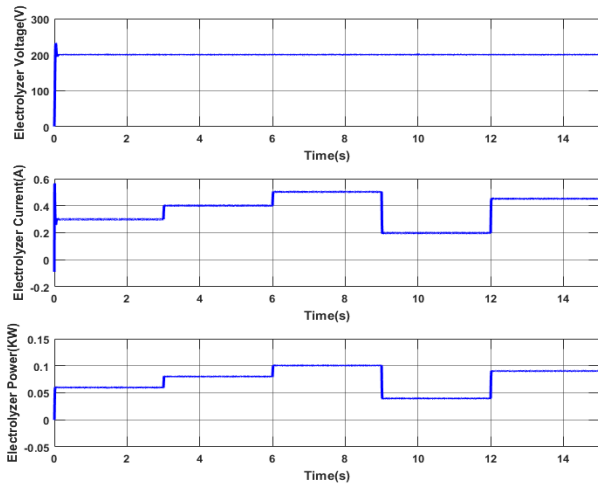


(a)

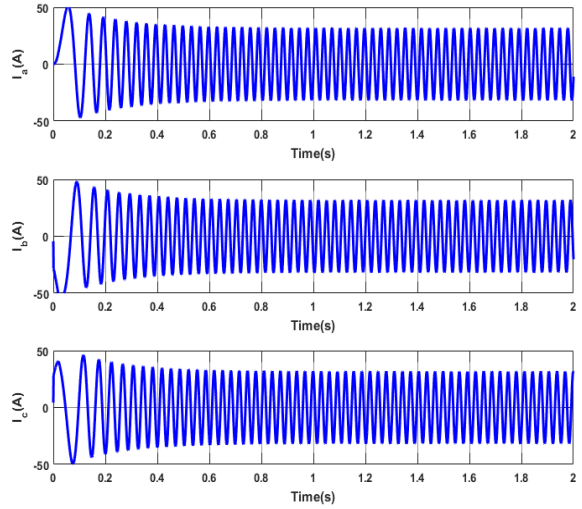


(b)

Fig 17. Fuel Cell Voltage and current (a) FC output voltage and power (b) FC converter output voltage, current and power

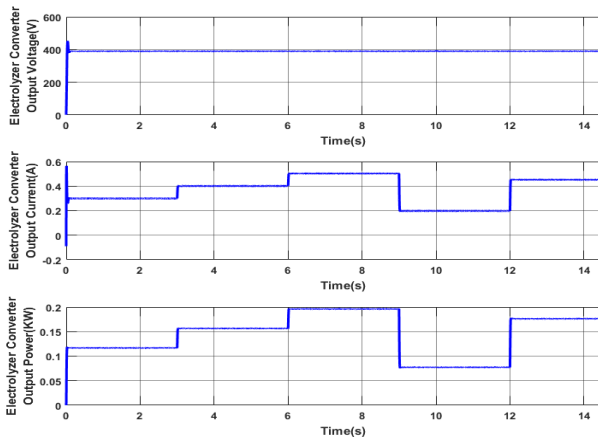


(a)



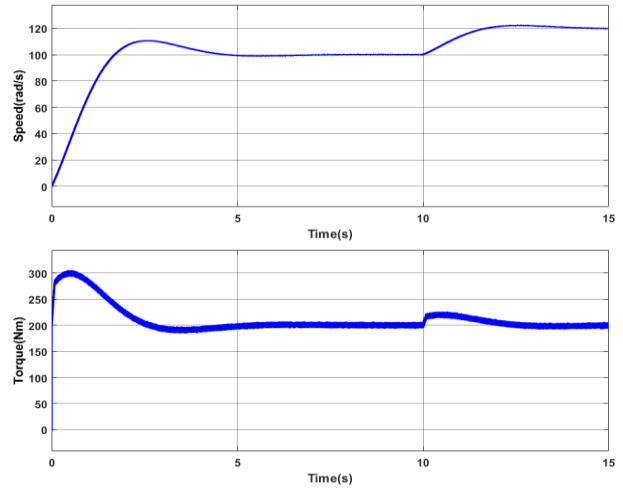
(b)

Fig 19. QBBC input voltage and output voltage (b) Motor Stator Currents during Starting with PI control

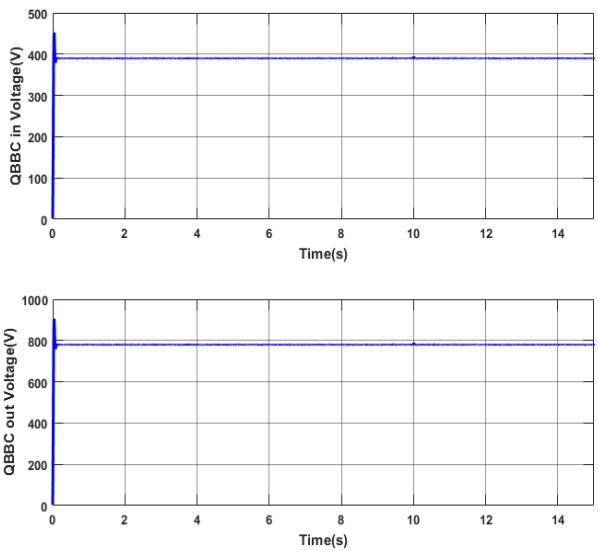


(b)

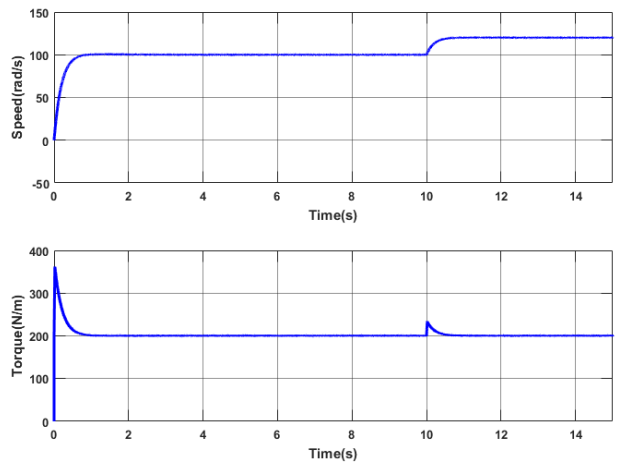
Fig 18. Electrolyzer Voltage and current (a) Electrolyzer voltage, current and power (b) Electrolyzer converter input voltage, current and power



(a)



(a)



(b)

Fig 20. Motor Speed and Torque (a) with PI Control (b) with Proposed Control

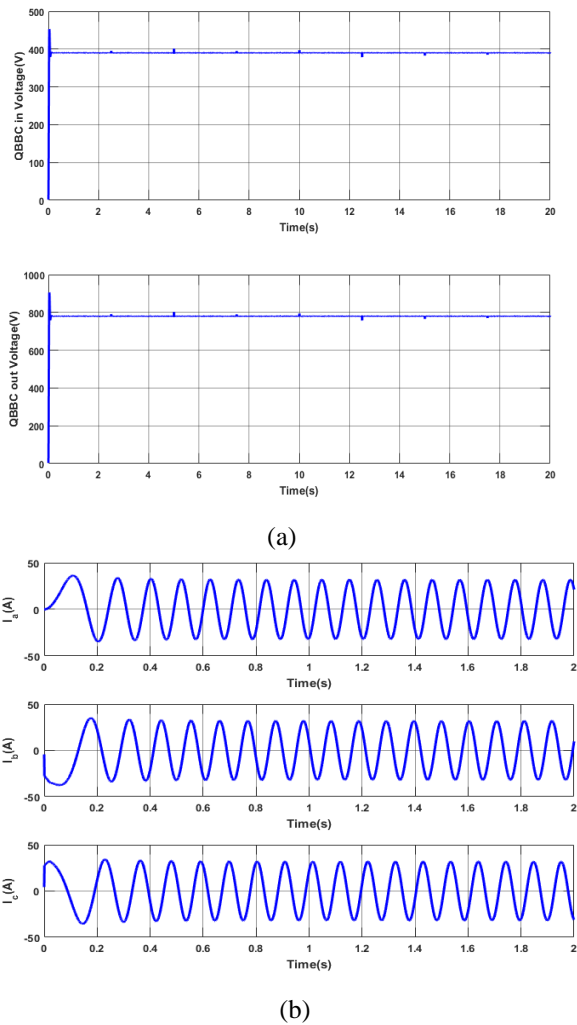


Fig 21. (a) QBBC input voltage and output voltage
(b) Motor Stator Currents

Case 3

Under constant irradiance conditions of 1000 W/m², the speed of the vehicle drive experiences the following variations: it rises from 30 rad/s to 50 rad/s at 2.5 seconds, then rises to 100 rad/s at the 5th second, further climbs to 120 rad/s at the 7.5 second, then reaches 150 rad/s at the 10th second, subsequently drops to 100 rad/s at the 12.5 second, decreases to 70 rad/s at the 15th second, and finally reduces to 50 rad/s at the 17.5 second. Figure 21(a) depicts the input and output voltages of the QBBC converter. Ensuring that the converter's output voltage stays at 780V is a critical requirement for the vehicle drive inverter. Figure 21 illustrates the motor speed and torque for both PI control and the proposed control approach. Figure 23(a) shows the output voltage, current, and power of the PV cell, while Figure 23(b) illustrates the output voltage, current, and power of the fuel cell. Motor active and reactive power are depicted in Figure 24.

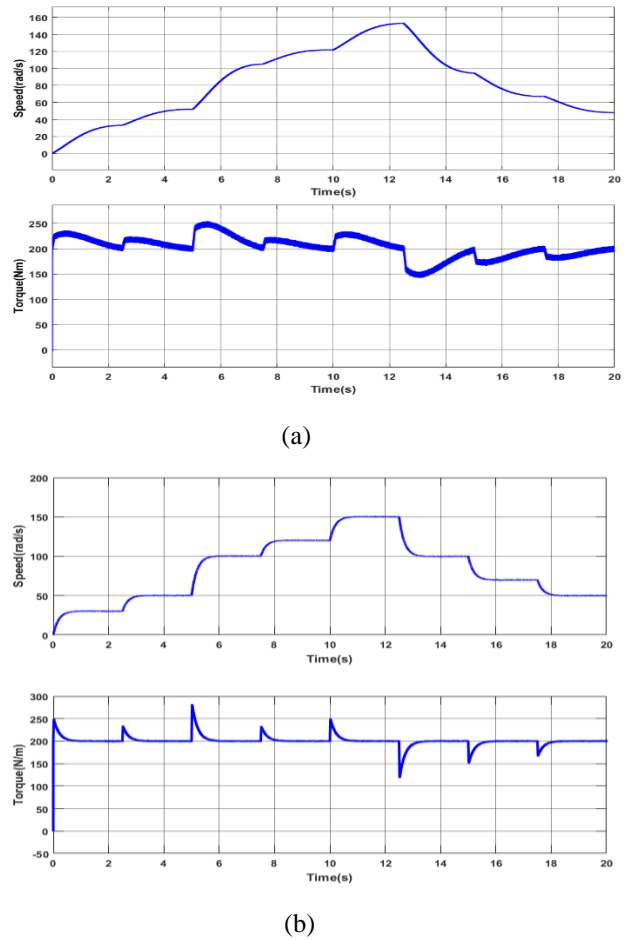
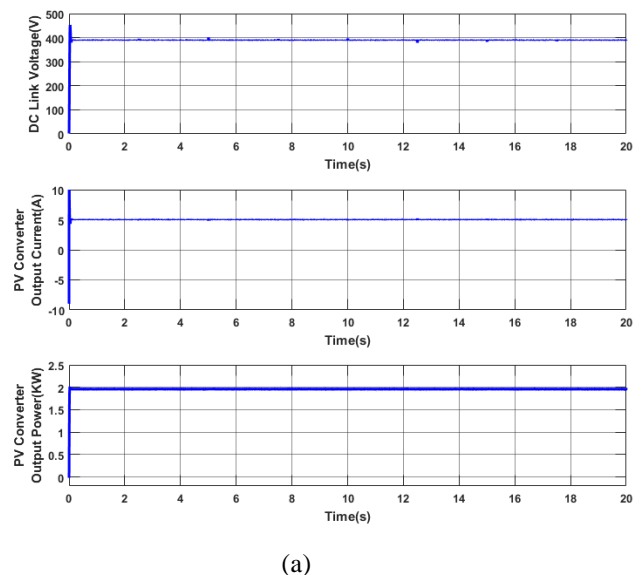
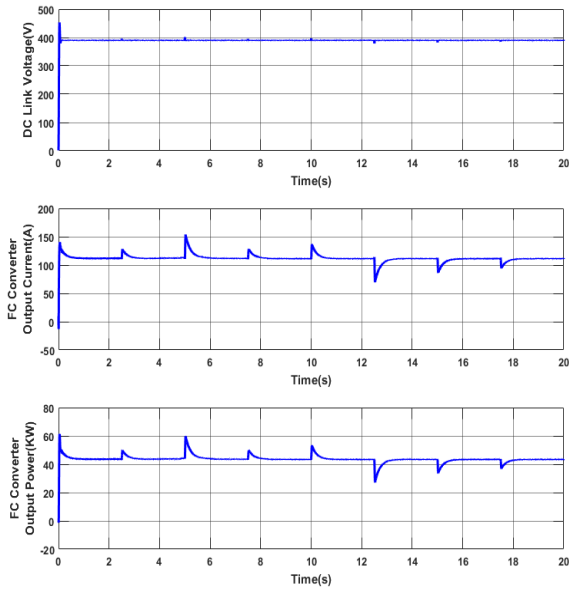


Fig 22. Motor Speed and Torque (a) with PI control
(b) with proposed control



(a)



(b)

Fig 23. (a) PV converter output voltage, current and power, (b) FC converter output voltage, current and power

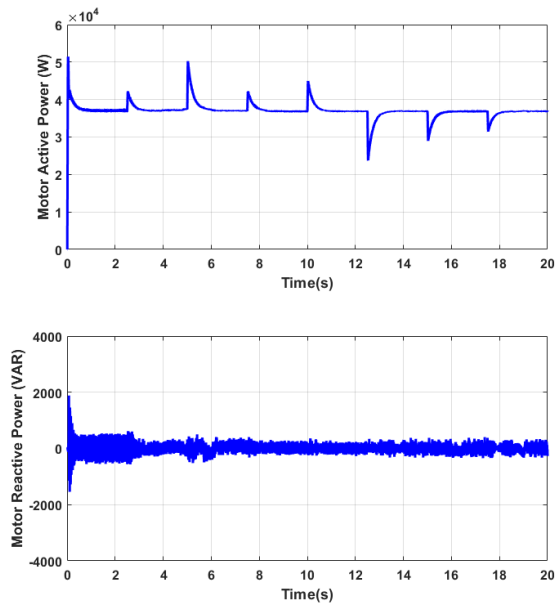
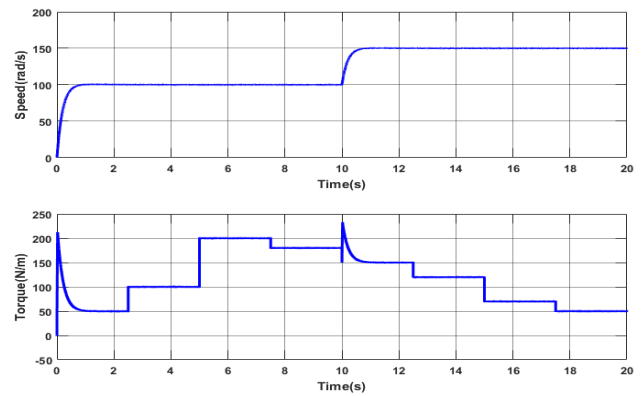


Fig 24. Motor Input active and reactive power with proposed control

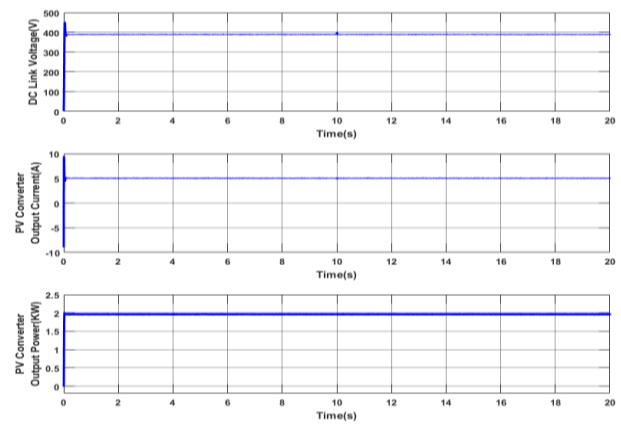
CASE4:

In this, it considers a sudden change in speed and varying load torque. The reference speed is initially increased from 100 rad/sec to 150 rad/sec at the 10-second mark. Simultaneously, the load torque experiences variations. It increased from 50 Nm to 100 Nm at 2.5 seconds, further raised to 200 Nm at the 5th second, followed by a decrease to 180 Nm at 7.5 seconds, and then to 150 Nm at the 10th second. Then, the load torque steadily decreases to 120 Nm at the

12.5-second mark, further dropping to 70 Nm at the 15th second, and ultimately reaching 50 Nm at the 17.5-second mark. The speed and torque of the vehicle drive are visually depicted in Figure 25(a). Figure 25(b) shows the output voltage, current, and power of the PV cell, while Figure 26(a) illustrates the corresponding data for the fuel cell. The performance of motor active and reactive power is depicted in Figure 27.

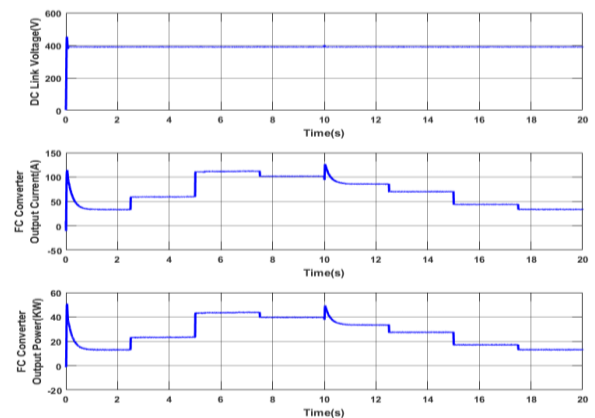


(a)

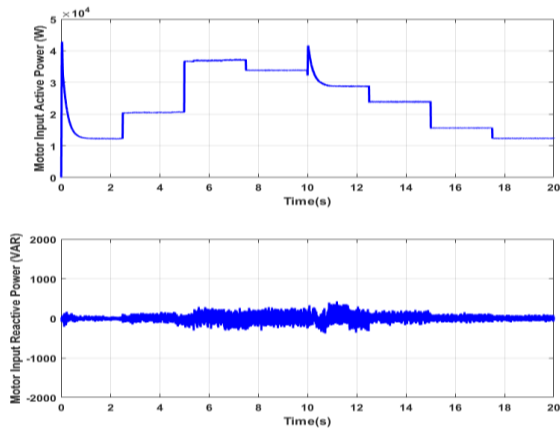


(b)

Fig 25. (a) Motor Speed and Torque. (b) PV converter output voltage, current and power



(a)



(b)

Fig 26. (a) FC converter output voltage, current and power, (b) Motor Input active and reactive power

7. Conclusion

This paper introduces an EV configuration featuring an innovative ANN Model Predictive Control (MPC) system. The setup combines a fuel cell, electrolyzer, and a PV cell on board. The on-board PV cell serves to complement the fuel cell by providing additional power when there is abundant irradiation to generate energy. Electrical energy is converted into chemical energy through an electrolyzer. A Quadratic Bidirectional Buck/Boost Converter is used to match the source voltage with the DC side voltage of the inverter in the vehicle drive. The PV system improves power extraction from the PV panel by utilizing the Incremental Conductance MPPT algorithm. The QBBC converters include an external voltage and internal current control loop to regulate and increase the voltage supplied by the sources. The motor speed is controlled using the innovative ANN MPC strategy, which eliminates the need for weighting factors. Additionally, this paper introduces a novel approach for predictive torque control of AC machines, deviating from traditional methods that rely on weighting factors. The motor speed is estimated using an ANN estimator. The equation for predicting the stator current is defined and adjusted based on the control procedure and the construction of the ANN accordingly. To assess the performance of the suggested configuration, simulations were conducted, considering changes in the reference speed and variations in irradiation. The simulation results show that the motor's reference speed is effectively tracked. In comparison to the conventional PI controller, the ANN MPC approach to enhances speed tracking concerning peak overshoot, rise time, and steady-state error.

References

- [1] Fantin Irudaya Raj, E., and M. Appadurai. "Internet of things-based smart transportation system for smart cities." *Intelligent Systems for Social Good: Theory and Practice*. Singapore: Springer Nature Singapore, 2022. 39-50.
- [2] Selmi, Tarek, Ahmed Khadhraoui, and Adnen Cherif. "Fuel cell-based electric vehicles technologies and challenges." *Environmental Science and Pollution Research* 29.52 (2022): 78121-78131..
- [3] Taghizad-Tavana, Kamran, et al. "A comprehensive review of electric vehicles in energy systems: Integration with renewable energy sources, charging levels, different types, and standards." *Energies* 16.2 (2023): 630.
- [4] Olabi, A. G., et al. "Battery electric vehicles: Progress, power electronic converters, strength (S), weakness (W), opportunity (O), and threats (T)." *International Journal of Thermofluids* 16 (2022): 100212.
- [5] Conway, G., Joshi, A., Leach, F., García, A. and Senecal, P.K., 2021. A review of current and future powertrain technologies and trends in 2020. *Transportation Engineering*, 5, p.100080.
- [6] Li, Yunwu, Xueyan Huang, Dexiong Liu, Mingfeng Wang, and Junjie Xu. "Hybrid energy storage system and energy distribution strategy for four-wheel independent-drive electric vehicles." *Journal of Cleaner Production* 220 (2019): 756-770.
- [7] Taghizad-Tavana, K., Alizadeh, A.A., Ghanbari-Ghalehjouhi, M. and Nojavan, S., 2023. A comprehensive review of electric vehicles in energy systems: Integration with renewable energy sources, charging levels, different types, and standards. *Energies*, 16(2), p.630.
- [8] G. Sree Lakshmi, S. Kamakshaiah and T. R. Das, "Closed loop PI control of PMSM for hybrid electric vehicle using three level diode clamped inverter for optimal efficiency," 2013 International Conference on Energy Efficient Technologies for Sustainability, Nagercoil, India, 2013, pp. 754-759, doi: 10.1109/ICEETS.2013.6533479.
- [9] De Melo, Hugo Neves, Joao Pedro F. Trovao, Paulo G. Pereirinha, Humberto M. Jorge, and Carlos Henggeler Antunes. "A controllable bidirectional battery charger for electric vehicles with vehicle-to-grid capability." *IEEE Transactions on Vehicular Technology* 67, no. 1 (2017): 114-123.
- [10] Yong, J. Y., Ramachandaramurthy, V. K., Tan, K. M., & Mithulanathan, N. (2015). A review on the state-of-the-art technologies of electric vehicles, its impacts and prospects. *Renewable and sustainable energy reviews*, 49, 365-385.

- [11] Hannan, M.A., Al-Shetwi, A., Begum, R.A., Young, S.E., Hoque, M.M., Ker, P., Mansur, M. and Alzaareer, K., 2020. The value of thermal management control strategies for battery energy storage in grid decarbonization: Issues and recommendations. *Journal of Cleaner Production*, 276, p.124223.
- [12] Latha, K. Sree, and M. Lakshmi Swarupa. "Design and implementation of power conditioning for distribution network V2G to electric vehicle and DC charging system." AIP Conference Proceedings. Vol. 2269. No. 1. AIP Publishing, 2020.
- [13] Kurien, C., Srivastava, A.K. and Molere, E., 2020. Emission control strategies for automotive engines with scope for deployment of solar based e-vehicle charging infrastructure. *Environmental Progress & Sustainable Energy*, 39(1), p.13267.
- [14] Kong, W., Luo, Y., Feng, G., Li, K., & Peng, H. (2019). Optimal location planning method of fast charging station for electric vehicles considering operators, drivers, vehicles, traffic flow and power grid. *Energy*, 186, 115826.
- [15] Bhasin, J. and Srivastava, N., A STUDY OF SELECT VARIABLES IMPACTING BUYING BEHAVIOUR OF ELECTRIC CARS IN INDIA.
- [16] Haider, S. W., Zhuang, G., & Ali, S. (2019). Identifying and bridging the attitude-behavior gap in sustainable transportation adoption. *Journal of Ambient Intelligence and Humanized Computing*, 10, 3723-3738.
- [17] Grin, J., Rotmans, J., & Schot, J. (2010). *Transitions to sustainable development: new directions in the study of long term transformative change*. Routledge.
- [18] Fathabadi, Hassan. "Combining a proton exchange membrane fuel cell (PEMFC) stack with a Li-ion battery to supply the power needs of a hybrid electric vehicle." *Renewable energy* 130 (2019): 714-724.
- [19] Peng FZ, Shen M, Holland K. Application of Z-source inverter for traction drive of fuel cell—Battery hybrid electric vehicles. *IEEE Transactions on Power Electronics*. 2007 May 7;22(3):1054-61.
- [20] Wu, X., Aviquzzaman, M. and Lin, Z., 2015. Analysis of plug-in hybrid electric vehicles' utility factors using GPS-based longitudinal travel data. *Transportation Research Part C: Emerging Technologies*, 57, pp.1-12.
- [21] Omer, Abdeen Mustafa. "Energy, environment and sustainable development." *Renewable and sustainable energy reviews* 12, no. 9 (2008): 2265-2300.
- [22] Mac Kinnon, M.A., Brouwer, J. and Samuelsen, S., 2018. The role of natural gas and its infrastructure in mitigating greenhouse gas emissions, improving regional air quality, and renewable resource integration. *Progress in Energy and Combustion science*, 64, pp.62-92.
- [23] Luo, Y., Wu, Y., Li, B., Qu, J., Feng, S. P., & Chu, P. K. (2021). Optimization and cutting-edge design of fuel-cell hybrid electric vehicles. *International Journal of Energy Research*, 45(13), 18392-18423.
- [24] Ellis, M. W., Von Spakovsky, M. R., & Nelson, D. J. (2001). Fuel cell systems: efficient, flexible energy conversion for the 21st century. *Proceedings of the IEEE*, 89(12), 1808-1818.
- [25] Manoharan, Y., Hosseini, S.E., Butler, B., Alzahrani, H., Senior, B.T.F., Ashuri, T. and Krohn, J., 2019. Hydrogen fuel cell vehicles; status and future prospect. *Applied Sciences*, 9(11), p.2296.
- [26] G. Divya, Venkata Padmavathi S., "Design and Modeling of Hybrid Electric Vehicle Powered by Solar and Fuel Cell Energy with Quadratic Buck/Boost Converter," *WSEAS Transactions on Circuits and Systems*, vol. 22, pp. 41-54, 2023, DOI:10.37394/23201.2023.22.7
- [27] Ates, Y., Erdinc, O., Uzunoglu, M. and Vural, B., 2010. Energy management of an FC/UC hybrid vehicular power system using a combined neural network-wavelet transform based strategy. *International journal of hydrogen energy*, 35(2), pp.774-783.
- [28] Thounthong, P., Chunkag, V., Sethakul, P., Davat, B., & Hinaje, M. (2009). Comparative study of fuel-cell vehicle hybridization with battery or supercapacitor storage device. *IEEE transactions on vehicular technology*, 58(8), 3892-3904.
- [29] F. A. Himmelstoss, A. Iz and H. L. Votzi, "Quadratic bidirectional buck-boost converter," 2020 International Symposium on Power Electronics, Electrical Drives, Automation and Motion (SPEEDAM), Sorrento, Italy, 2020, pp. 738-743, doi: 10.1109/SPEEDAM48782.2020.9161829.